research papers

CrossMark

Structure of the catalytic phosphatase domain of MTMR8: implications for dimerization, membrane association and reversible oxidation

Ki-Young Yoo,[a] Ji Young Son,[a] Jee Un Lee,[a] Woori Shin,[a] Dong-Won Im,[a] Seung Jun Kim,[b] Seong Eon Ryu[c]* and Yong-Seok Heo[a]*

[a]Department of Chemistry, Konkuk University, 1 Hwayang-dong, Gwangjin-gu, Seoul 143-701, Republic of Korea, [b]Medical Proteomics Research Center, Korea Research Institute of Bioscience and Biotechnology, 111 Gwahangno, Yuseong-gu, Daejeon 305-806, Republic of Korea, and [c]Department of Bio Engineering, Hanyang University, Seongdong-gu, Seoul 133-791, Republic of Korea. *Correspondence e-mail: ryuse@hanyang.ac.kr, ysheo@konkuk.ac.kr

Myotubularin-related proteins are a large family of phosphoinositide phosphatases; their activity, stability and subcellular localization are regulated by dimeric interactions with other members of the family. Here, the crystal structure of the phosphatase domain of MTMR8 is reported. Conformational deviation of the two loops that mediate interaction with the PH-GRAM domain suggests that the PH-GRAM domain interacts differently with the phosphatase domain of each MTMR member. The protein exists as a dimer with twofold symmetry, providing insight into a novel mode of dimerization mediated by the phosphatase domain. Structural comparison and mutation studies suggest that Lys255 of MTMR8 interacts with the substrate diacylglycerol moiety, similar to Lys333 of MTMR2, although the positions of these residues are different. The catalytic activity of the MTMR8 phosphatase domain is inhibited by oxidation and is reversibly reactivated by reduction, suggesting the presence of an oxidation-protective intermediate other than a disulfide bond owing to the absence of a cysteine within a disulfide-bond distance from Cys338.

1. Introduction

Phosphatidylinositol (PtdIns) is a major eukaryotic membrane lipid composed of diacylglycerol and a D-*myo*-inositol head group. The conversion of PtdIns to its derivatives mediates a variety of cellular processes such as defining intracellular organelle identity, cell signalling, proliferation, membrane trafficking and cytoskeleton organization (Balla, 2013; De Matteis & Godi, 2004; Di Paolo & De Camilli, 2006; Odorizzi *et al.*, 2000). The D3, D4 and D5 positions on the inositol ring of PtdIns can be phosphorylated to seven derivatives, known as phosphoinositides (PIs; Supplementary Fig. S1). In response to environmental changes, cellular PI levels are regulated by several phospholipases, lipid kinases and phosphatases. Among the seven phosphoinositides, phosphatidylinositol 3-phosphate [PtdIns(3)P] and phosphatidylinositol 3,5-bisphosphate [PtdIns(3,5)P$_2$] control autophagy and endosomal trafficking events by recruiting effector proteins that contain phosphoinositide-binding modules such as pleckstrin homology (PH), epsin N-terminal homology (ENTH) and Fab1p/YOTB/Vac1p/EEA1 (FYVE) domains (Ferguson *et al.*, 2009; Friant *et al.*, 2003; Huang *et al.*, 2011; Lemmon, 2003; Nicot & Laporte, 2008; Robinson & Dixon, 2006).

The myotubularin-related proteins (MTMRs) are a large family of conserved proteins that dephosphorylate PtdIns(3)P and PtdIns(3,5)P$_2$ to yield PtdIns and PtdIns(5)P, respectively
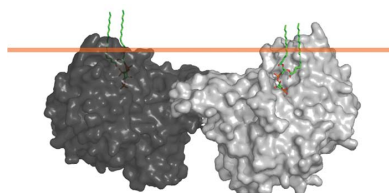
(Blondeau *et al.*, 2000). The myotubularin gene (*MTM1*) was initially identified as a gene that is mutated in most patients with X-linked myotubular myopathy, a fatal congenital muscle disease characterized by centrally placed nuclei in muscle fibres and defective muscle-cell development (Laporte *et al.*, 1996, 2000; Spiro *et al.*, 1966). Since the initial identification of *MTM1*, 13 additional myotubularin-related genes, named *MTMR1–13*, have been identified (Laporte *et al.*, 2003; Lepichon *et al.*, 2010; Nandurkar *et al.*, 2001; Senderek *et al.*, 2003; Tosch *et al.*, 2006; Wishart *et al.*, 2001). Mutations in MTMR2 and MTMR13 cause Charcot–Marie–Tooth disease type 4B, a neurodegenerative disease characterized by axonal degeneration and myelin outfolding (Azzedine *et al.*, 2003; Bolino *et al.*, 2000, 2001). In addition to these two diseases, several MTMRs have been reported to be associated with human diseases, including cancers, obesity and metabolic syndrome, epilepsy and Creutzfeld–Jakob disease (Hendriks & Pulido, 2013).

The members of the MTMR family share a common structural core consisting of a PH-GRAM domain, a catalytic phosphatase domain and a coiled-coil domain (Begley & Dixon, 2005). Additional domains such as FYVE, PH, DENN and PDZ-binding domains are also contained in each member of the MTMR family (Supplementary Fig. S1). These similar but different domain constructs suggest that the myotubularin proteins are not redundant and have unique functions by regulating a specific pool of PtdIns(3)P and PtdIns(3,5)P_2 dephosphorylation within cells (Clague & Lorenzo, 2005; Laporte *et al.*, 1998, 2003; Taylor & Dixon, 2003). Varying tissue expression and subcellular localization also contribute to the unique function of each myotubularin protein (Berger *et al.*, 2003; Kim *et al.*, 2002, 2003; Lorenzo *et al.*, 2005; Xue *et al.*, 2003).

Among the 14 myotubularin-related proteins, eight (MTM1, MTMR1–4 and MTMR6–8) possess the catalytic activity of dephosphorylating PtdIns(3)P and PtdIns(3,5)P_2 *via* the conserved active-site Cys-X_5-Arg motif characteristic of protein tyrosine phosphatases (PTPs; Alonso *et al.*, 2004; Vergne & Deretic, 2010). The remaining members (MTMR5 and MTMR9–13) are catalytically inactive as they contain inherent missense substitutions at the conserved Cys and Arg residues within the active-site Cys-X_5-Arg motif (Laporte *et al.*, 2003). These inactive members form specific heterodimeric interactions with the active myotubularin proteins to regulate their activity, substrate specificity, stability and subcellular localization (Berger *et al.*, 2006; Kim *et al.*, 2003; Mochizuki & Majerus, 2003; Nandurkar *et al.*, 2003; Zou *et al.*, 2009). Several homodimeric interactions between active members have also been reported (Lorenzo *et al.*, 2006). In all of these myotubularin interactions the coiled-coil domain provides a critical binding interface for dimerization (Berger *et al.*, 2003; Kim *et al.*, 2003). However, MTMR3 and MTMR4 mutants with the coiled-coil motif deleted can form homodimeric or heterodimeric interactions, suggesting that another domain provides an auxiliary dimeric interface (Lorenzo *et al.*, 2006). The catalytic activity of MTM1 is enhanced by the formation of a heptameric ring structure, suggesting the presence of additional interdomain contacts, as the single coiled-coil domain is not sufficient to form the ring structure (Schaletzky *et al.*, 2003). Although the canonical interaction between coiled-coil domains has been well characterized, no structural information has been reported on the putative interaction of domains other than the coiled-coil domain in MTMRs.

The crystal structure of MTMR2 encompassing the PH-GRAM and catalytic phosphatase domains has been reported (Begley *et al.*, 2003). The PH-GRAM domain is actually part of a larger motif with a PH-domain fold, suggesting that it may function as a PI-binding module that targets its host proteins to specific cell membranes, as PH domains do in many proteins. The catalytic domain is similar to PTPs but is significantly larger, with an additional SET-interaction domain (SID), which is a putative protein–protein interaction mediator. The crystal structures of MTMR2 in complex with PtdIns(3)P or PtdIns(3,5)P_2 have led to the elucidation of the substrate specificity of MTMRs, which have wider and deeper active sites than those of phosphoprotein-specific PTPs, providing selectivity for the larger headgroup of PIs (Begley *et al.*, 2006). The specificity for PtdIns(3)P or PtdIns(3,5)P_2 is determined by specific interactions of the headgroups, and the binding of PIs phosphorylated at other positions would be prohibited by steric collision with the MTMRs.

Here, we describe the crystal structure of the catalytic phosphatase domain of human MTMR8 and discuss the implications of this structure in the context of mutagenesis, GST pull-down, cross-linking and reversible oxidation data to enhance our understanding of the dimerization, membrane association, substrate recognition and redox regulation of MTMRs.

2. Experimental procedures

2.1. Protein expression and purification

The sequence encoding the catalytic phosphatase domain of MTMR8 (amino acids 122–505) and the PH-GRAM domain (amino acids 1–102) were subcloned into pET-21a (Novagen); site-directed mutagenesis of the phosphatase domain was performed with the QuikChange Kit (Agilent Technologies) and was confirmed by DNA sequencing. The wild-type and mutant proteins were expressed in *Escherichia coli* as C-terminally 6×His-tagged proteins and were purified from the soluble fraction of the cell lysate by metal-affinity chromatography followed by anion-exchange and gel-filtration chromatography. For the GST pull-down experiment, the phosphatase domain of MTMR8 was also expressed as a fusion protein with an N-terminal GST. Expression and purification protocols, including buffer compositions, are provided in the Supporting Information.

2.2. Crystallization and data collection

The purified protein (C388S) was concentrated to 5 mg ml^{-1} in buffer consisting of 20 m*M* Tris pH 8.0, 200 m*M* NaCl, 5 m*M* DTT. The concentrated protein was crystallized by the hanging-drop method with a reservoir solution

Table 1
Data-collection and structure-refinement statistics.

Values in parentheses are for the outer resolution shell.

Data collection	
Synchrotron	PLS
Beamline	7A
Wavelength (Å)	1.0000
Space group	$P2_12_12_1$
Unit-cell parameters (Å)	$a = 69.57$, $b = 77.188$, $c = 197.79$
Resolution (Å)	2.80 (2.85–2.80)
Unique reflections	26992
Muliplicity	5.8 (6.0)
Completeness (%)	100.0 (100.0)
Average $I/\sigma(I)$	17.0 (2.6)
R_{merge}† (%)	8.8 (48.9)
Structure refinement	
Resolution (Å)	41.6–2.80
R_{cryst}‡ (%)	17.7
R_{free}§ (%)	24.7
No. of protein atoms	6126
No. of ligand atoms	20
No. of water molecules	163
Wilson B factor (Å^2)	48.0
Average B factor (Å^2)	
Protein atoms	47.75
Ligand atoms	49.21
Water molecules	44.96
R.m.s.d.¶	
Bonds (Å)	0.009
Angles (°)	1.2
Ramachandran plot	
Outliers (%)	0.13
Favoured (%)	94.43

† $R_{merge} = \sum_{hkl} \sum_i |I_i(hkl) - \langle I(hkl) \rangle| / \sum_{hkl} \sum_i I_i(hkl)$ for the intensity $I_i(hkl)$ of i observations of reflection hkl. ‡ $R_{cryst} = \sum_{hkl} ||F_{obs}| - |F_{calc}|| / \sum_{hkl} |F_{obs}|$, where F_{obs} and F_{calc} are the observed and calculated structure factors, respectively. § R_{free} is the R factor calculated using 5% of the reflections data chosen randomly and omitted from the start of refinement. ¶ Root-mean-square deviations from ideal geometry.

consisting of 10 mM N-(2-acetamido)iminodiacetic acid, 1.0 M ammonium phosphate dibasic pH 6.5 at 20°C. The crystals were cryocooled in liquid nitrogen after soaking in a cryo-protectant (20% glycerol added to the crystallization buffer). X-ray diffraction data were collected at 100 K on beamline 7A of the Pohang Light Source (PLS), Republic of Korea. The crystals belonged to space group $P2_12_12_1$, with unit-cell parameters $a = 69.57$, $b = 77.188$, $c = 197.79$ Å and with two molecules in the asymmetric unit and a solvent content of 60.2%. X-ray diffraction data were collected to a resolution of 2.80 Å. Data were indexed, integrated, scaled and merged using *DENZO* and *SCALEPACK* from the *HKL*-2000 software package (Otwinowski & Minor, 1997).

2.3. Structural determination and refinement

The structure was solved by the molecular-replacement (MR) method using *Phaser* (McCoy *et al.*, 2005; Storoni *et al.*, 2004) from the *CCP*4 suite (http://www.ccp4.ac.uk; Winn *et al.*, 2011) with the coordinates of the catalytic phosphatase domain of MTMR2 (PDB entry 1lw3; Begley *et al.*, 2003) as a search model. After rigid-body refinement and restrained refinement by *REFMAC*5 (Murshudov *et al.*, 2011), the model was manually revised using *Coot* (Emsley & Cowtan, 2004) and was further refined using *REFMAC*5. The final model contained two MTMR8 molecules consisting of residues 125–

503, four phosphate ions and 186 water molecules, with an R and R_{free} of 0.177 and 0.247, respectively. Statistics of the data collection and structure refinement are presented in Table 1.

2.4. GST pull-down

The purified GST-tagged phosphatase domain of MTMR8 was incubated with 6×His-tagged phosphatase or PH-GRAM domain for 3 h at 4°C. Glutathione-agarose beads (GE Healthcare Life Sciences) were added to the proteins and incubated for a further 1 h. The beads were washed five times with buffer consisting of 20 mM Tris pH 8.0, 200 mM NaCl, 5 mM DTT and boiled in SDS–PAGE sample buffer. Proteins were resolved by SDS–PAGE, and Western blotting was carried out with anti-His-tag antibody (Sigma–Aldrich).

2.5. Glutaraldehyde-mediated cross-linking

The purified wild-type and mutant MTMR8 proteins were incubated at room temperature for 15 min after adding 0.1% glutaraldehyde. The cross-linked proteins were separated by SDS–PAGE and stained with Coomassie Blue dye.

2.6. Measurement of phosphatase activity

The catalytic activity of the phosphatase domain of MTMR8 was measured by monitoring the liberated free phosphate ions using malachite green dye. Phosphatase assays were performed in 80 μl reaction mixtures consisting of 20 mM Tris pH 8.0, 200 mM NaCl, 5 mM DTT, 0–150 μM diC8PtdIns(3,5)P$_2$ (Cayman Chemical), 1 μg MTMR8 protein (wild type or mutants). The reaction mixture was incubated at 30°C for 10 min and quenched by adding 20 μl malachite green reagent (a 1:1 mixture of 40 mM ammonium molybdate in 6 M HCl and 1.5 mM malachite green with 0.27% polyvinyl alcohol). The mixture was allowed to develop for 30 min and the absorbance was measured at 650 nm using a plate reader. The Michaelis–Menten kinetics parameters K_m and k_{cat} were determined from a direct fit of the data to the Lineweaver–Burk equation. All experiments were performed in triplicate.

2.7. Reversible oxidation and reactivation of MTMR8

The solution of the purified wild-type MTMR8 phosphatase domain contained 5 mM DTT during purification; this was removed by exchanging the buffer into 20 mM Tris pH 8.0, 200 mM NaCl on a HiTrap Desalting Column (GE Healthcare Life Sciences). Increasing amounts of H$_2$O$_2$ (0.02–20 mM) were added to MTMR8 (800 nM) and incubated for 10 min at 20°C. After removing H$_2$O$_2$ by buffer exchange, oxidized samples were reactivated by DTT (5 mM). The phosphatase activities of the oxidized and reactivated proteins (300 nM) were measured using the malachite green phosphatase activity assay. During the assay of the oxidized protein, DTT was not included in the reaction mixture. All experiments were performed in triplicate. The activity of each sample was compared with untreated reduced enzyme, which was set as 100%.

3. Results

3.1. Overall structure of the MTMR8 catalytic domain and its structural comparison with MTMR2

The catalytic domain of human MTMR8 (amino acids 122–505) with an inactivating mutation (C338S) in the Cys-X_5-Arg motif was crystallized using ammonium phosphate as a precipitant and its structure was determined by molecular replacement using the structure of the catalytic domain of MTMR2 (PDB entry 1lw3). The MTMR8 phosphatase

domain contains 15 α-helices and a seven-stranded β-sheet, and its core structure is similar to that of other Cys-X_5-Arg motif-based phosphatase structures (Fig. 1a). Two strong electron-density peaks corresponding to free phosphate ions, perhaps originating from the crystallization condition, were apparent in the active site and one of them was surrounded by the consensus Cys-X_5-Arg motif, indicating the position of this electron density is the D3 site of the bound substrate PIs. The amino-acid sequences of the phosphatase domains of MTMR8 and MTMR2 are highly conserved (45% identity) and their
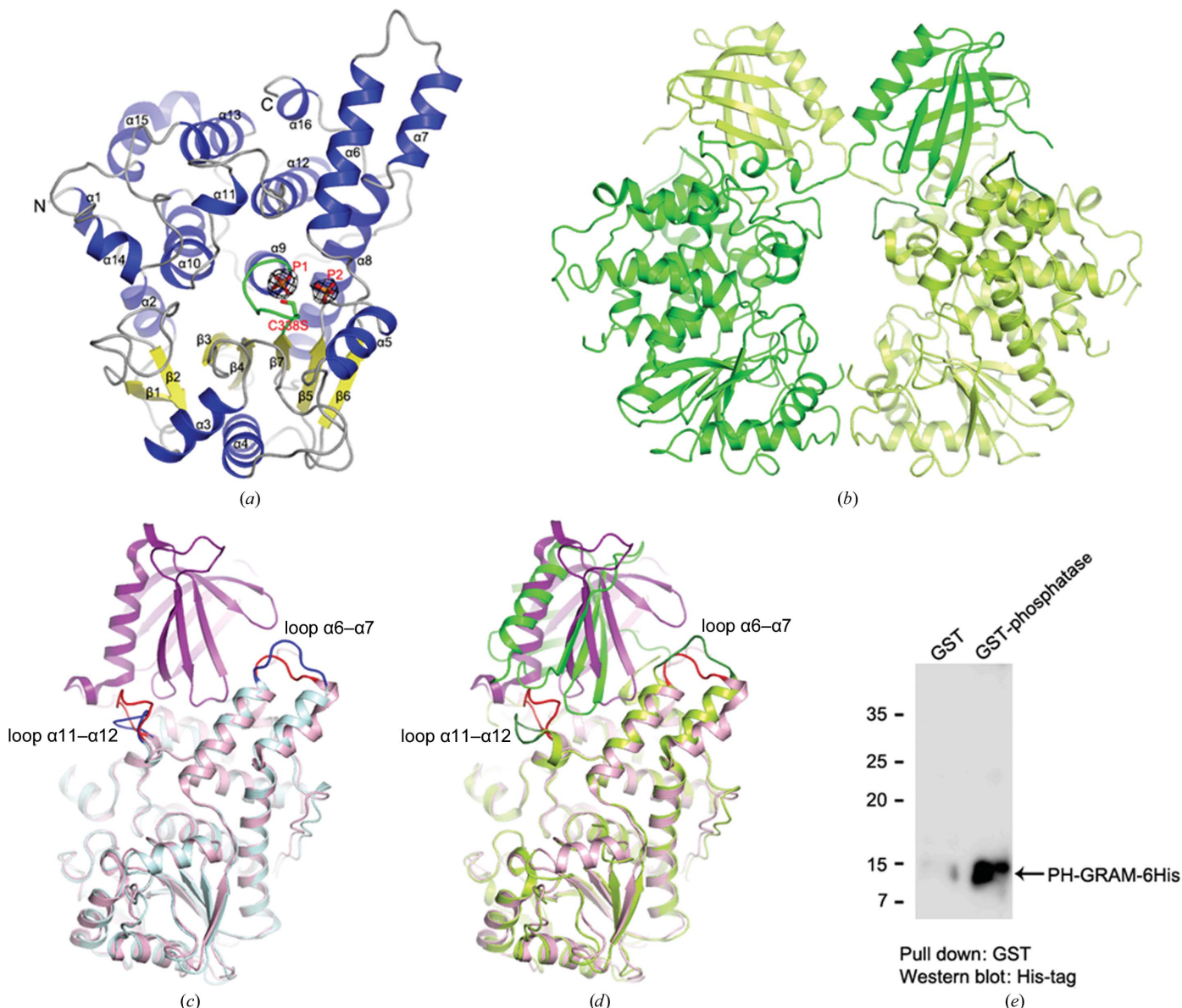

Figure 1
Crystal structure of the phosphatase domain of MTMR8. (a) Overall view of the MTMR8 structure (amino acids 122–505). The Cys-X_5-Arg motif is shown in green. The mutated residue C338S is shown as a stick model. Two phosphates (P1 and P2) in the active site are shown with the corresponding $F_o - F_c$ map contoured at 4σ. (b) Domain swapping of MTMR6. The green and pale green MTMR6 molecules are related by crystallographic symmetry. (c) Structural comparison of the phosphate domain of MTMR8 (cyan) with that of MTMR2 (pale purple). The PH-GRAM domain of MTMR2 is shown in purple. The $\alpha6$–$\alpha7$ and $\alpha11$–$\alpha12$ loops of MTMR8 and MTMR2 are shown in blue and red, respectively. (d) Structural comparison of MTMR6 (green) with MTMR2 (purple). The phosphatase domains of MTMR6 and MTMR2 are shown in lime and pale purple, respectively. The $\alpha6$–$\alpha7$ and $\alpha11$–$\alpha12$ loops of MTMR6 and MTMR2 are shown in dark green and red, respectively. All structure figures were produced with *PyMOL* (http://www.pymol.org). (e) Purified GST-tagged phosphatase domain of MTMR8 was incubated with 6×His-tagged PH-GRAM domain of MTMR8. As a control, GST was incubated with 6×His-tagged PH-GRAM domain of MTMR8. Each protein was pulled down by glutathione-agarose beads. Coprecipitated proteins were resolved by SDS–PAGE and detected by Western blotting with anti-His antibody.

structures can be easily superimposed. Least-squares comparison of the MTMR8 and MTMR2 catalytic domains showed that their overall structures are very similar (root-mean-square deviation of 1.2 Å). The most divergent regions are loop $\alpha6$–$\alpha7$ and loop $\alpha11$–$\alpha12$, which form the extensive PH-GRAM/phosphatase domain binding interface in the structure of MTMR2 (Fig. 1c). However, the conformations of these two loops in MTMR8 would not be able to retain the PH-GRAM/phosphatase domain interaction as they do in MTMR2 owing to the lack of structural complementarity and amino-acid sequence homology (Supplementary Fig. S2). In the crystal structure of MTMR2, the PH-GRAM domain is connected to the phosphatase domain by a 20-residue linker and is apposed to the phosphatase domain via the interface to form a compact globular structure (Begley et al., 2003). A previous deuterium-exchange mass-spectrometry (DXMS) study showed that the segments in the PH-GRAM/phosphatase domain interface are among the least solvent-accessible areas; thus, the extensive interaction between the two domains is a fixed property of MTMR2 in solution and the position of the PH-GRAM domain relative to the active site would be optimal for contact with PIs in membranes (Begley et al.,

2006). The crystal structure of MTMR6 (PDB entry 2yf0, Structural Genomics Consortium, unpublished work) shows that this protein dimerizes with a crystallographic symmetry-related neighbouring molecule by swapping the PH-GRAM and phosphatase domains (Fig. 1b). It is unclear whether this domain swapping can occur in solution; however, the two domains of each MTMR6 make an extensive binding interface and the binding orientation between the two domains is very different from that in MTMR2 (Fig. 1d). A GST pull-down experiment showed that the separately expressed PH-GRAM and phosphatase domains of MTMR8 also bind to each other (Fig. 1e). Of course, the $\alpha6$–$\alpha7$ and $\alpha11$–$\alpha12$ loops of MTMR8 may adapt their conformation to fit the potential interaction between the two domains. The amino-acid sequence alignment shows that the residues of loops $\alpha6$–$\alpha7$ and $\alpha11$–$\alpha12$ of MTMR8 are more conserved in MTMR6 and MTMR7 than in the other active MTMRs (Supplementary Fig. S2). Therefore, the PH-GRAM domain of MTMR8 is expected to interact with the phosphatase domain differently from MTMR2, as it does in MTMR6. The PH-GRAM/phosphatase domain interface would determine the position and orientation of the PH-GRAM domain relative to the membrane. The diversity of the PH-GRAM/phosphatase domain interfaces suggests that the PH-GRAM domains have unique functions in each member of the MTMR family.

3.2. Substrate recognition and membrane association of MTMR8

Sequence analysis revealed that the residues involved in hydrogen bonding or ionic inter-actions during substrate binding by MTMR2 are conserved in all active MTMRs, suggesting that all active MTMRs have the same substrate specificity and a similar binding mode (Supplementary Fig. S2). To investigate the substrate-binding mode of MTMR8, its structure was super-posed onto the structure of MTMR2 in complex with the lipid substrates PtdIns(3)P or PtdIns(3,5)P_2. As expected, the two free phosphate ions in the active site of MTMR8 were posi-tioned at the D1 and D3 sites of the substrate PI and the substrate molecule precisely docked into the active site of MTMR8 (Fig. 2a). The D3 phosphate is surrounded by hydrogen bonds to the backbone amide groups and
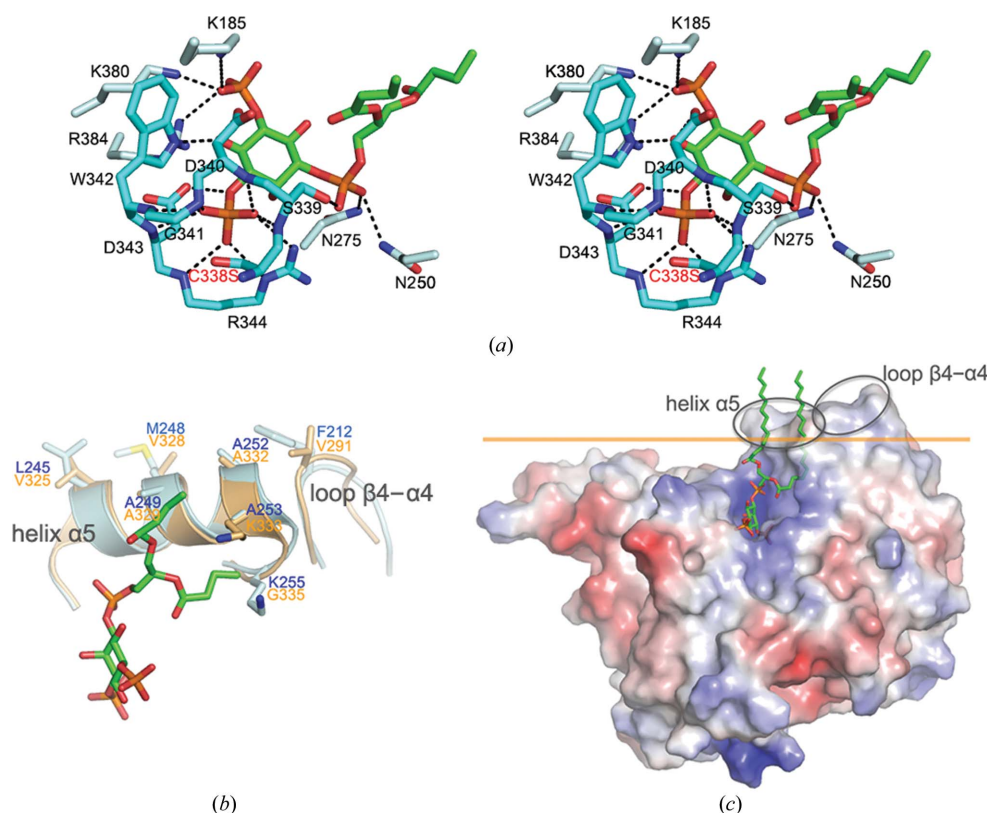

Figure 2
Interactions of MTMR8 with the substrate PI and membrane bilayer. (a) Hypothetical model of PtdIns(3,5)P_2 in the active site of MTMR8 with its D1 and D3 phosphate groups superimposed onto the phosphate ions shown in Fig. 1(a). The model is shown in atomic colours with C atoms of PtdIns(3,5)P_2 in green, the Cys-X_5-Arg motif in blue and other residues in cyan. Hydrogen bonds are shown as dotted lines. (b) Putative residues for membrane association. The $\alpha5$ helix and $\beta4$–$\alpha4$ loop of MTMR8 (cyan) are superimposed onto those of MTMR2 (pale orange) in complex with PtdIns(3,5)P_2 (green). (c) Suggested location of the membrane plane for MTMR8 in complex with PtdIns(3,5)P_2 (green). MTMR8 is shown as an electrostatic potential surface and the putative interaction plane with the membrane is shown as an orange line. The locations of the $\alpha6$ helix and $\beta4$/$\alpha4$ loop are indicated as ellipses.
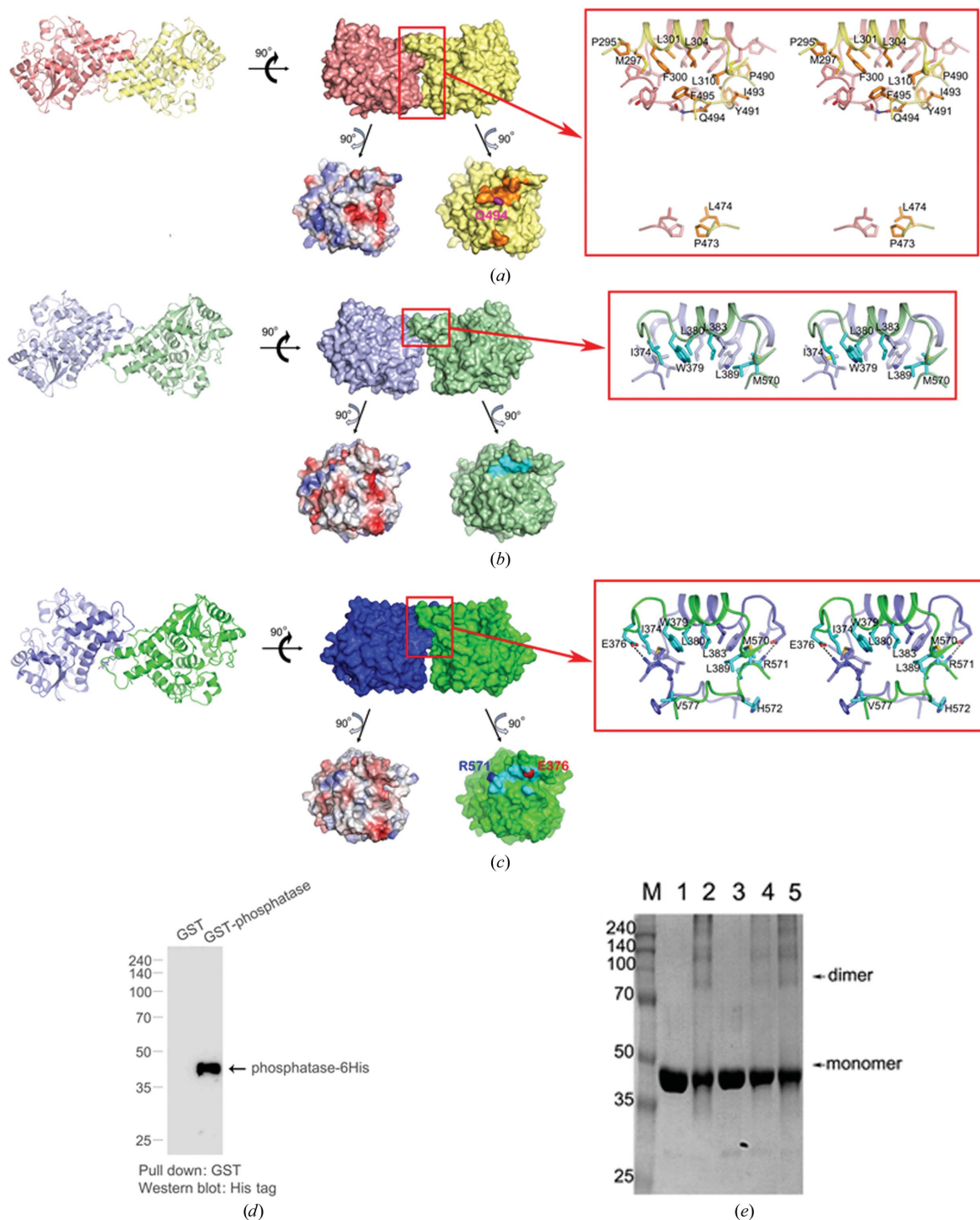
Figure 3
Phosphatase domain-mediated dimerization of MTMR. (*a*) The dimer structure of MTMR8 is shown as a cartoon model and surface model in different orientations. The dimer interface is shown as an electrostatic potential surface; the residues involved in the hydrophobic interaction are shown in orange and Gln494 in purple in the surface model. A close-up view of the dimer interaction is shown in the red box. The residues for the dimer interaction are labelled on one protomer of the dimer of MTMR8 for clarity. The hydrogen bond of Gln494 is shown as a dotted line. (*b*) The dimer structure of open-form MTMR2 (PDB entry 1m7r). The residues involved in the hydrophobic interaction are coloured cyan. (*c*) The dimer structure of closed-form MTMR2 (PDB entry 1lw3). The residues involved in the hydrophobic interaction are coloured cyan, Arg571 blue and Glu376 red in the surface model. The hydrogen bonds between Arg571 and Glu376 are shown as dotted lines. (*d*) Purified GST-tagged phosphatase domain of MTMR8 was incubated with 6×His-tagged phosphatase domain of MTMR8. As a control, GST was incubated with 6×His-tagged phosphatase domain of MTMR8. Each protein was pulled down by glutathione-agarose beads. Coprecipitated proteins were resolved by SDS–PAGE and detected by Western blotting with anti-His antibody. (*e*) Glutaraldehyde-mediated cross-linking of the phosphatase domain of MTMR8. The cross-linked proteins were separated by SDS–PAGE. Lane M, protein size marker (labelled in kDa); lane 1, wild type without glutaraldehyde; lane 2, wild type cross-linked by 0.1% glutaraldehyde; lane 3, mutant (F200A/L301A/L304A) cross-linked by 0.1% glutaraldehyde; lane 4, mutant (Q494E) cross-linked by 0.1% glutaraldehyde; lane 5, mutant (P473A/L474A) cross-linked by 0.1% glutaraldehyde

side chains of the Cys-X_5-Arg motif containing Cys338, Ser339, Asp340, Gly341, Trp342, Asp343 and Arg344. As in the case of Asp422 in MTMR2, Asp343 of MTMR8 is within hydrogen-bonding distance of the scissile O atom of the D3 phosphate, indicating that it functions as a general acid/base during catalysis. The D1 phosphate interacts with the side chains of Asn250, Asn275 and Ser339, and the D5 phosphate forms ionic interactions with Lys380 and Arg384. The bulky side chain of Trp342 forms a hydrogen bond to the 4-hydroxyl group of the inositol ring and prohibits the binding of any PIs phosphorylated at the D4 position owing to steric collision with the D4 phosphate, accounting for the substrate selectivity of the active MTMRs.

In the crystal structure of MTMR2, the diacylglycerol moiety of the substrate PI makes nonspecific, hydrophobic interactions with the α-helix which contains Lys333 and surface-exposed, hydrophobic residues (Val325, Val328, Ala329 and Ala332; Fig. 2b). A previous DXMS study revealed that this α-helix is a highly solvent-accessible region and may insert into the membrane bilayer to access the substrate PIs (Begley et al., 2006). The aliphatic chain of Lys333 was thought to contribute to substrate-binding affinity by van der Waals interaction with the diacylglycerol moiety. However, the corresponding residue in MTMR6, MTMR7 and MTMR8 is an alanine, which would reduce the interaction owing to its small size (Supplementary Fig. S2). Instead, Lys255 of MTMR8 is conserved in MTMR6 and MTMR7, although the corresponding residue is a glycine in other

MTMRs. A K255A mutation reduced the phosphatase activity (k_{cat}/K_m) by 66%, indicating that Lys255 in MTMR8 also contributes to the substrate-binding affinity, like Lys333 in MTMR2 (Supplementary Fig. S3). The A253K mutation enhanced the k_{cat}/K_m value by 49%, suggesting that Lys255 of MTMR8 and Lys333 of MTMR2 mediate substrate recognition and membrane association of the $\alpha5$ helix in a similar manner, although they occupy different positions in the active site (Fig. 2b). The residues of active MTMRs at the same position as Phe212 in the $\beta4$–$\alpha4$ loop of MTMR8 are hydrophobic and very close to the $\alpha5$ helix (Supplementary Fig. S2). In addition, Phe212 is surface-exposed, like the hydrophobic residues in the $\alpha5$ helix, suggesting that the hydrophobic residue in the $\beta4$–$\alpha4$ loop may insert into the membrane bilayer with the $\alpha5$ helix despite the lack of interaction with the substrate PIs (Fig. 2c).

3.3. Dimer interface of the phosphatase domain

The phosphatase domain of MTMR8 exists as a dimer in the asymmetric unit of the crystal with noncrystallographic twofold symmetry. The buried area of the dimerization is 2068 Å^2 and the dimerization interaction is mediated by hydrophobic residues in the $\alpha6$–$\alpha7$ loop, the $\alpha7$ helix, the $\alpha15$–$\alpha16$ loop and the $\alpha16$ helix and a hydrogen bond between the side chains of Gln494 from neighbouring molecules (Fig. 3a). Although the coiled-coil domain is thought to provide a major interface for the dimerization of MTMRs, several MTMR
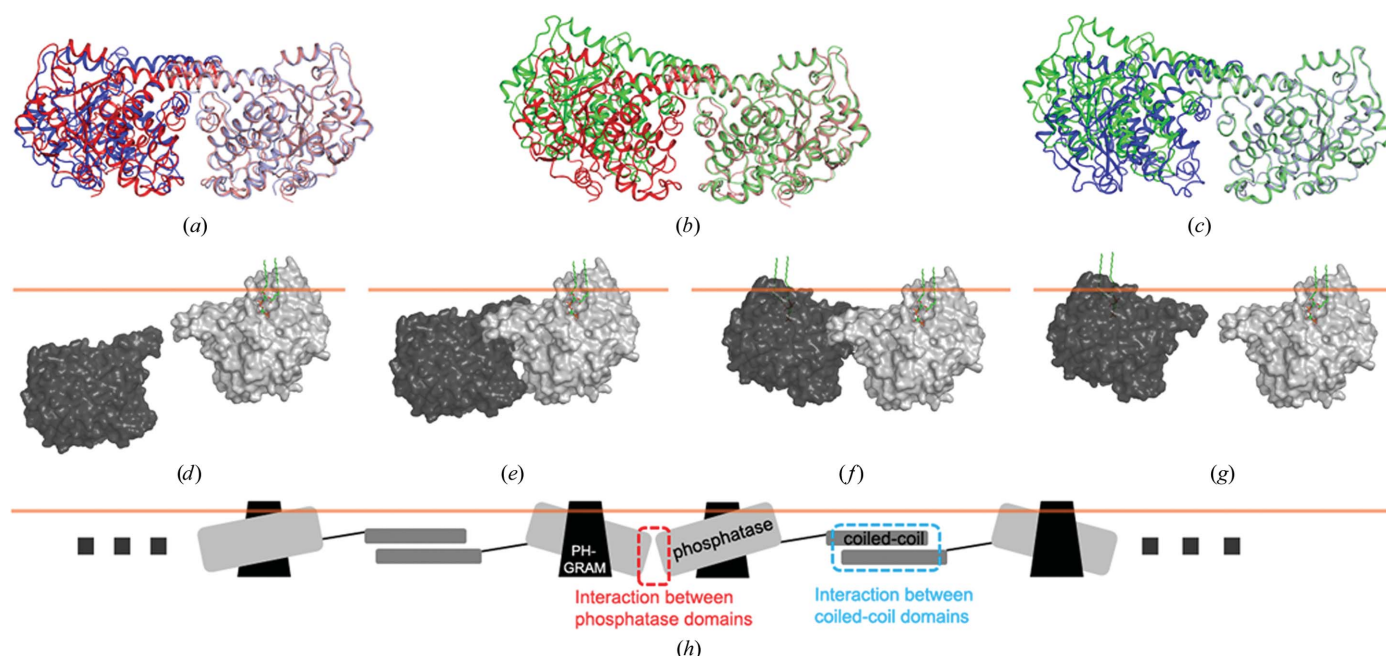

Figure 4
Proposed mechanism of activity enhancement by dimerization. (a) The dimer structures of MTMR8 (red) and the closed form of MTMR2 (blue). A protomer of MTMR8 (pale red) was superimposed onto that of MTMR2 (pale blue). (b) The dimer structures of MTMR8 (red) and the open form of MTMR2 (green). A protomer of MTMR8 (pale red) was superimposed onto that of MTMR2 (pale green). (c) The dimer structures of the open-form MTMR2 (green) and closed-form MTMR2 (blue). A protomer of each dimer was superimposed. (d–g) Proposed mechanism of phosphatase domain-mediated dimerization of MTMRs. (d) An MTMR protein (grey) binds to a membrane PI and another (black) in the cytosol. (e) Two protomers interact in the closed dimeric form. (f) Both protomers bind to membrane PIs in the open dimeric form. (g) Two protomers dissociate to recruit other MTMR proteins. (h) Hypothetical model of the oligomeric state of MTMRs by the interactions of phosphatase domain-mediated and coiled-coil domain-mediated dimerization.

members can form a dimer in the absence of the coiled-coil domain, suggesting that another domain may be involved in dimerization (Lorenzo *et al.*, 2006). A GST pull-down experiment verified that the MTMR8 phosphatase domain can interact with itself (Fig. 3*d*). We hypothesized that the dimer interface in the MTMR8 crystal could represent the additional dimer interface, as the size of the buried area is not negligible. Interestingly, similar dimeric interfaces are also found in the crystals of MTMR2 belonging to different space groups (Begley *et al.*, 2003). Selenomethionine-substituted MTMR2
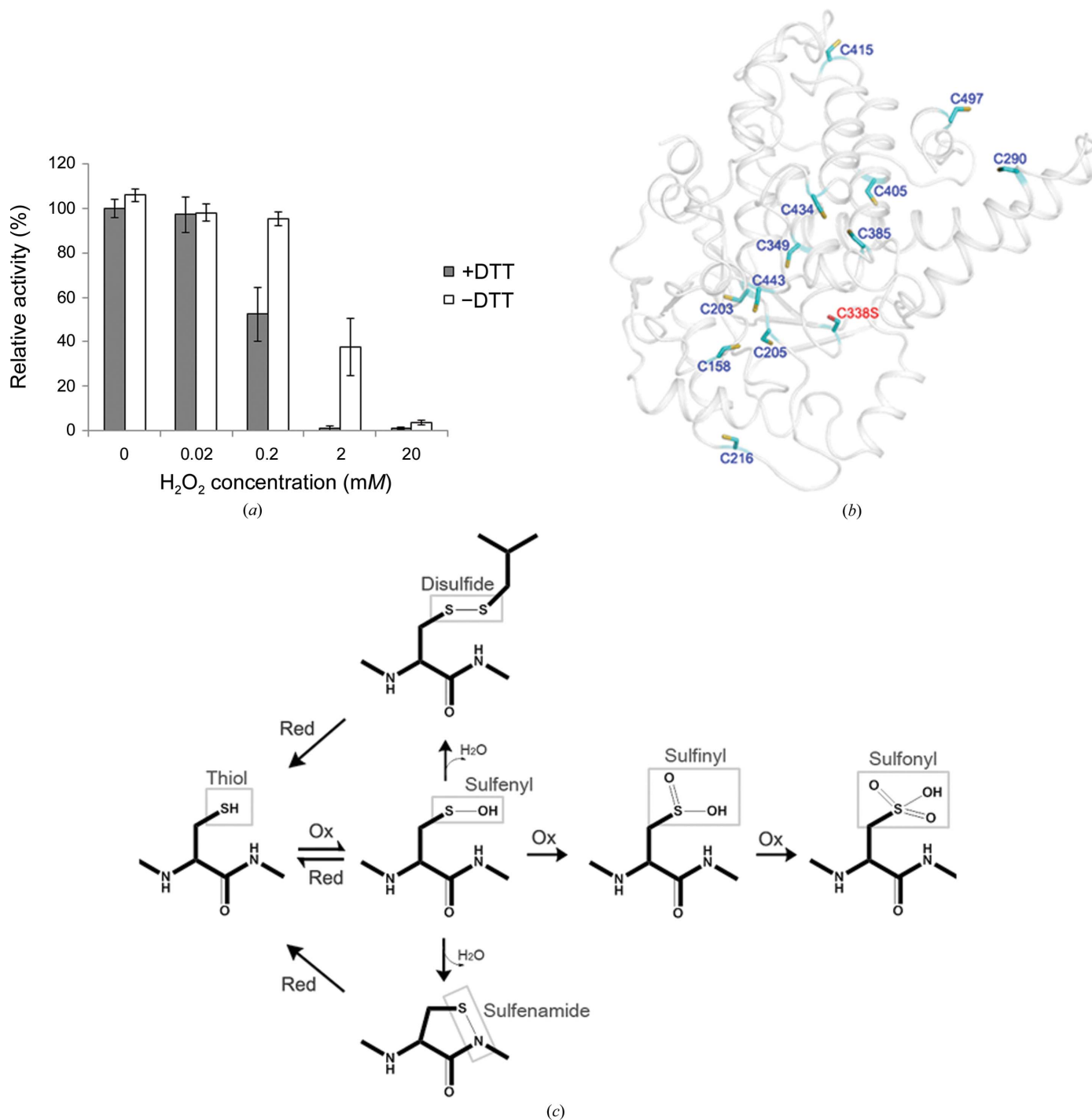

Figure 5
Reversible oxidation of MTMR8. (*a*) The phosphatase domain of MTMR8 was incubated with increasing concentrations of H_2O_2. Aliquots of H_2O_2-treated MTMR8 were used in the phosphatase assay following buffer exchange, without or with DTT, to observe the inactivation and reactivation of the enzyme. The results are presented as means + standard deviations of triplicate determinations. (*b*) All Cys residues of the phosphatase domain of MTMR8 are shown. (*c*) Oxidative modification of cysteines. The thiol group (–SH) is oxidized to a sulfenyl group (–SOH) by ROS in cells. The –SOH group forms a disulfide bond with another Cys or a sulfenamide bond with an N atom in the protein backbone. The disulfide and sulfenamide bonds can be reduced by antioxidants in cells. However, –SOH can also be further oxidized to a sulfinyl group (–SO$_2$H) and a sulfonyl group (–SO$_3$H); neither of these groups can be reduced in the normal intracellular environment.

(PDB entry 1m7r) crystals belonged to space group $C2$ and contained two MTMR2 molecules in the asymmetric unit with a buried area of 1182 Å^2 in the dimer interface. The hydrophobic residues in the $\alpha 7$ helix provided the main interface for dimerization and the relative positions of the two protomers resulted in a very open dimeric form owing to this small buried area (Figs. 3b, 4a, 4b and 4c). Native MTMR2 crystals (PDB entry 1lw3) formed in space group $P4_12_12$ with one molecule in the asymmetric unit, but a similar mode of dimeric interaction was found with a crystallographic symmetry-related neighbouring molecule. In this case, additional interactions are made as the side chain of Arg571 changed its conformation and made a salt bridge to Glu376 of the neighbouring molecule (Fig. 3c). In addition, His572 and Val577 provide a van der Waals interaction for dimerization. As a result of these additional interactions, the buried area could be increased to 1601 Å^2 and the dimer could have a closed form, similar to the dimeric form of the MTMR8 structure (Figs. 4a, 4b and 4c). To verify that this crystallographic dimer interface mediates protein dimerization in solution, the oligomeric states of the wild type and several mutants of the phosphatase domain of MTMR8 were probed by glutaraldehyde-mediated cross-linking (Fig. 3e). The wild-type protein was partially cross-linked as a dimer or a higher oligomer in solution and the mutations affected the oligomeric state. The F300G/L301G/L304G mutant was not cross-linked at all, perhaps owing to loss of the hydrophobic interaction or a change in the secondary structure of the $\alpha 7$ helix. These hydrophobic residues are conserved in all active MTMRs and the interaction mediated by these residues is common to the three cases of crystallographic dimer interactions, suggesting that the $\alpha 7$ helix serves a critical interface for dimerization of MTMRs. The Q494E mutant attenuated cross-linking owing to a loss of the hydrogen bond between the side chains of the two neighbouring Gln494 residues; this residue is not conserved in other MTMRs, indicating that this hydrogen bond is of secondary importance for dimerization and the interaction is unique to MTMR8. In the case of MTMR2, the ionic interaction between Glu376 and Arg571 of the neighbouring molecule would act as an auxiliary interaction for dimerization instead of the hydrogen bond of Glu494 in MTMR8. Finally, the P473G/L474G mutation did not affect cross-linking, indicating that the hydrophobic interaction of Pro473 and Leu474 contributes little, if anything, to the dimerization of MTMR8 and is merely a consequence of dimerization. In conclusion, these cross-linking data confirm that the crystallographic dimer interface indeed mediates dimerization of the phosphatase domain of MTMR8 in solution and that this interaction could be a general mode of dimerization of MTMRs owing to the conservation of the hydrophobic residues in the $\alpha 7$ helix (Supplementary Fig. S2).

3.4. Reversible oxidation and inactivation of MTMR8

Reactive oxygen species (ROS) are continuously generated during aerobic respiration in mitochondria and have been regarded as harmful molecules that damage various bio-molecules inside cells by oxidation, contributing to the process of aging and various diseases (Finkel & Holbrook, 2000). However, recent studies have shown that ROS can act as physiological messengers that mediate intracellular signalling, and several ROS effector proteins, which are oxidized sensitively and reversibly by ROS, play important roles in ROS-mediated signalling (Kawahara et al., 2007). Among the ROS effector proteins, protein-tyrosine phosphatases (PTPs) are of particular interest as they commonly possess the active-site cysteine of the consensus Cys-X_5-Arg motif, which is essential for catalytic activity and is highly sensitive to oxidation by ROS (Ostman et al., 2011; Tanner et al., 2011). The low pK_a of the central cysteine owing to its surrounding electronic environment in the active site renders PTPs susceptible to inactivation by ROS-induced oxidation (Zhang & Dixon, 1993). The first step of oxidation of the thiol moiety of the catalytic Cys results in formation of a sulfenyl moiety, which can be reverted to a thiol upon reduction by various antioxidants in the cell (Tonks, 2005). However, the sulfenyl moiety is unstable and is further oxidized to the sulfinyl and sulfonyl moieties, which is an irreversible process in most cases (Fig. 5c). To avoid irreversible oxidation, the sulfenyl moiety can be converted into more stable forms, including a sulfenamide or a disulfide bond (Sivaramakrishnan et al., 2010). Crystallographic studies of PTP1B and RPTPα revealed that the reversibly oxidized forms of these enzymes contain an intramolecular cyclic sulfenamide bond, which induces a conformational rearrangement of the catalytic site P-loop (Salmeen et al., 2003; van Montfort et al., 2003; Yang et al., 2007). Crystallographic and biochemical studies of KAP, Cdc25, PRL and PTEN showed that these phosphatases are inactivated by reversible oxidation through the formation of a disulfide bond from the catalytic Cys to a proximal Cys residue (Buhrman et al., 2005; Fauman et al., 1998; Funato & Miki, 2014; Lee et al., 2002; Leslie et al., 2003; Sohn & Rudolph, 2003; Song et al., 2001). The fact that active members of the MTMR family also possess the consensus Cys-X_5-Arg motif led us to examine whether MTMR8 can be inactivated by oxidation and reactivated by reduction. Oxidation by the increasing H_2O_2 concentration eliminated the phosphatase activity of MTMR8, but reduction of the oxidized protein with dithiothreitol (DTT) reactivated the protein to some extent, suggesting that the biological function of MTMR8 can be regulated by ROS-mediated oxidation and that a protective intermediate of MTMR8 for reversible reduction may exist (Fig. 5a).

To investigate whether the catalytic Cys can form an intramolecular disulfide bond, we checked the positions of the Cys residues in the structure of the phosphatase domain of MTMR8. The protein contains 12 Cys residues in addition to the catalytic Cys338, but none is within a disulfide-bond distance of Cys338 (Fig. 5b). In addition, the Cys residues are located on a secondary structure or a structurally well defined loop which forms several interactions with surrounding residues. Therefore, it is unlikely that dramatic structural changes occur to create an intramolecular disulfide bond between distant cysteines, which may bring a distantly located cysteine

into a constrained position, as this would be energetically unfavourable owing to collapse of the core structure. Several mass-spectrometric studies have shown that disulfide bond-mediated reversible oxidation in phosphatases requires an additional Cys residue near the catalytic Cys to create a disulfide bond without requiring a conformational change. SDS–PAGE under nonreducing conditions is a simple method to detect both intramolecular and intermolecular disulfide bonds. Proteins with an intramolecular disulfide bond generally have high mobility as they adopt a more compact conformation owing to the disulfide bond inside the protein. In contrast, intermolecular disulfide bonds slow migration owing to the increased size of the protein. Nonreducing SDS–PAGE of H_2O_2-oxidized wild-type and C338S-mutant MTMR8 with DTT produced no mobility shift, indicating an absence of intramolecular or intermolecular disulfide bonds (data not shown). It is therefore likely that the protective intermediate of MTMR8 for reversible redox reaction is an intramolecular cyclic sulfenamide bond, in which the S atom in the catalytic cysteine (Cys338) is covalently linked to the main-chain N atom of the adjacent residue. Alternatively, the sulfenyl form could retain its structure in the reversible oxidation despite its intrinsic instability. Of course, we cannot exclude the possibility of other mechanisms of redox regulation and intermediate formation in various Cys-X_5-Arg motif-based phosphatases. Further X-ray crystallography and mass-spectrometric studies will provide a complete picture of redox regulation in the MTMR family.

4. Discussion

Our structural study of the catalytic phosphatase domain of human MTMR8 suggests that the interaction between the PH-GRAM and phosphatase domains of MTMR8 deviates substantially from that of MTMR2 owing to the different structures of the $\alpha6$–$\alpha7$ and $\alpha11$–$\alpha12$ loops. In addition, the dimerization of MTMRs can be mediated by the phosphatase domain through interaction of the hydrophobic residues in the $\alpha7$ helix. The PH domain in many proteins is supposed to contribute to initial membrane recruitment of the host protein by binding phospholipids in the membrane. The PH-GRAM domain has the folding of the PH domain, and therefore is supposed to be involved in PI binding, although its function differs between MTMRs. The PH-GRAM domains of MTMR proteins also bind several different PIs with some specificity; however, the binding affinity is very low (less than 1 mM), suggesting that the membrane interaction mediated by the PH-GRAM domain must cooperate with other low-affinity interactions for functional binding of MTMRs to the membrane (Berger et al., 2003; Lorenzo et al., 2005; Tsujita et al., 2004).

Bioinformatics studies have shown that the PH-GRAM and phosphatase domains of active MTMRs are electrostatically polarized, with the positive charge localized to the membrane-proximal surface (Begley et al., 2006). The positive charge would mediate electrostatic interactions with the negatively charged headgroup of PIs in the membrane. In the crystal structure of MTMR2, the phosphatase and PH-GRAM domains form a tight interaction with a buried area of 1350 Å^2 per domain, suggesting that the PH-GRAM domain may not only help to recruit MTMR2 to the membrane but may also serve to position and orient the catalytic phosphatase domain optimally with respect to the PI substrate in the membrane owing to the size and rigidity of the PH-GRAM/phosphatase domain interface (Begley et al., 2003). However, the structures of MTMR8 and MTMR6 suggest that the modes of interaction between the PH-GRAM and phosphatase domain in MTMR6, MTMR7 and MTMR8 differ from that in MTMR2 or other active MTMRs. In MTMRs, phosphatase domain-mediated dimerization would also serve to orient the active site of the catalytic domain towards the bilayer in cooperation with the interaction between the PH-GRAM and phosphatase domains, as this dimerization makes the active sites of both protomers face in the same direction.

The glutaraldehyde-mediated cross-linking of the phosphatase domain of MTMR8 was only partial in solution and the protein was eluted as a monomer by gel-filtration chromatography during purification (data not shown), implying that the dimeric interaction through the phosphatase domain would be very weak and dependent on the protein concentration in solution. This weak interaction would have an advantage over stronger interactions such as the coiled-coil domain-mediated interaction in that the weak binding would have some intrinsic flexibility in the interaction and thus could easily change the relative orientation of the protomers in a dimer, enabling swift dissociation to exchange binding partners. For the membrane association of MTMRs, the $\alpha5$ helix and $\beta4$–$\alpha4$ loop would be partially inserted into a membrane bilayer during recognition and dephosphorylation of the substrate PIs. When one MTMR molecule binds to the substrate in a membrane, the putative dimer interface of the phosphatase domain is exposed to the cytosol; this interface helps to pull another MTMR molecule to the membrane to form a dimer (Fig. 4d). The initial binding mode would adopt the closed dimeric form to enhance the binding affinity for fast association (Fig. 4e). However, this closed form prevents simultaneous binding of both protomers to substrate PIs in the membrane; therefore, the dimer interaction changes to the open form (Fig. 4f). The change from the closed to the open dimeric form weakens the already weak dimer interaction, thereby facilitating dissociation and exposing the putative dimer interface to recruit another MTMR to form a new dimer in the vicinity of the membrane PIs (Fig. 4g). The $\alpha7$ helix, which is stabilized through intramolecular interaction with the $\alpha6$ helix, provides the key hydrophobic interaction for phosphatase domain-mediated dimerization of MTMR8. The $\alpha6$ and $\alpha7$ helices are unique to members of the MTMR family and are not included in the core structure shared by most other Cys-X_5-Arg motif-based phosphatases. The flexibility of the dimer interface caused by the weak interaction of the $\alpha7$ helix could also help to optimally orient the phosphatase domain with respect to the substrate PIs in the membrane by delicately swinging the dimer structure from a closed to an open form. In addition, the dimeric interaction by the phos-

phatase domain could enhance the catalytic activity of MTMRs as this dimerization makes the active sites of both protomers face the membrane bilayer, and thus facilitates recognition of the substrate PIs with an optimal orientation for catalysis. The catalytic activity of MTM1 is enhanced by the formation of a heptameric ring structure (Schaletzky *et al.*, 2003). The oligomeric state of MTMR could be mediated by alternating interactions of phosphatase domain-mediated and coiled-coil domain-mediated dimerization (Fig. 4h). The coiled-coil domain is supposed to be a part of an extended region of MTMRs and completely displaced from the catalytic phosphatase domain; thus, the coiled-coil domain-mediated interaction would be unable to induce structural changes in the active site and affect catalytic efficiency. However, any delicate structural change of the catalytic domain by phosphatase domain-mediated dimerization could easily be propagated to the active site, thereby subtly altering the active site into a more productive species for catalysis.

MTMR6 specifically inhibits the Ca^{2+}-activated K^+ channel KCa3.1 and this functional specificity is determined by the PH-GRAM and coiled-coil domains, which are required for co-localization of MTMR6 with KCa3.1 to the plasma membrane (Choudhury *et al.*, 2006). Thus, MTMR6 associates with the plasma membrane through two specific low-affinity interactions: between the coiled-coil domains on MTMR6 and KCa3.1 and between the PH-GRAM domain and PIs of the plasma membrane. Thus, membrane associations of MTMRs are likely to be cooperative processes involving several domains including the PH-GRAM, phosphatase and coiled-coil domains. At this time, we cannot exclude the possibility that other domains of MTMRs may contribute to membrane association by interacting with phospholipids or membrane-bound proteins.

References

Alonso, A., Sasin, J., Bottini, N., Friedberg, I., Friedberg, I., Osterman, A., Godzik, A., Hunter, T., Dixon, J. & Mustelin, T. (2004). *Cell*, **117**, 699–711.

Azzedine, H., Bolino, A., Taïeb, T., Birouk, N., Di Duca, M., Bouhouche, A., Benamou, S., Mrabet, A., Hammadouche, T., Chkili, T., Gouider, R., Ravazzolo, R., Brice, A., Laporte, J. & LeGuern, E. (2003). *Am. J. Hum. Genet.* **72**, 1141–1153.

Balla, T. (2013). *Physiol. Rev.* **93**, 1019–1137.

Begley, M. J. & Dixon, J. E. (2005). *Curr. Opin. Struct. Biol.* **15**, 614–620.

Begley, M. J., Taylor, G. S., Brock, M. A., Ghosh, P., Woods, V. L. & Dixon, J. E. (2006). *Proc. Natl Acad. Sci. USA*, **103**, 927–932.

Begley, M. J., Taylor, G. S., Kim, S.-A., Veine, D. M., Dixon, J. E. & Stuckey, J. A. (2003). *Mol. Cell*, **12**, 1391–1402.

Berger, P., Berger, I., Schaffitzel, C., Tersar, K., Volkmer, B. & Suter, U. (2006). *Hum. Mol. Genet.* **15**, 569–579.

Berger, P., Schaffitzel, C., Berger, I., Ban, N. & Suter, U. (2003). *Proc. Natl Acad. Sci. USA*, **100**, 12177–12182.

Blondeau, F., Laporte, J., Bodin, S., Superti-Furga, G., Payrastre, B. & Mandel, J.-L. (2000). *Hum. Mol. Genet.* **9**, 2223–2229.

Bolino, A., Lonie, L. J., Zimmer, M., Boerkoel, C. F., Takashima, H., Monaco, A. P. & Lupski, J. R. (2001). *Neurogenetics*, **3**, 107–109.

Bolino, A., Muglia, M., Conforti, F. L., LeGuern, E., Salih, M. A., Georgiou, D. M., Christodoulou, K., Hausmanowa-Petrusewicz, I., Mandich, P., Schenone, A., Gambardella, A., Bono, F., Quattrone, A., Devoto, M. & Monaco, A. P. (2000). *Nature Genet.* **25**, 17–19.

Buhrman, G., Parker, B., Sohn, J., Rudolph, J. & Mattos, C. (2005). *Biochemistry*, **44**, 5307–5316.

Choudhury, P., Srivastava, S., Li, Z., Ko, K., Albaqumi, M., Narayan, K., Coetzee, W. A., Lemmon, M. A. & Skolnik, E. Y. (2006). *J. Biol. Chem.* **281**, 31762–31769.

Clague, M. J. & Lorenzo, O. (2005). *Traffic*, **6**, 1063–1069.

Di Paolo, G. & De Camilli, P. (2006). *Nature (London)*, **443**, 651–657.

Emsley, P. & Cowtan, K. (2004). *Acta Cryst.* **D60**, 2126–2132.

Fauman, E. B., Cogswell, J. P., Lovejoy, B., Rocque, W. J., Holmes, W., Montana, V. G., Piwnica-Worms, H., Rink, M. J. & Saper, M. A. (1998). *Cell*, **93**, 617–625.

Ferguson, C. J., Lenk, G. M. & Meisler, M. H. (2009). *Hum. Mol. Genet.* **18**, 4868–4878.

Finkel, T. & Holbrook, N. J. (2000). *Nature (London)*, **408**, 239–247.

Friant, S., Pécheur, E.-I., Eugster, A., Michel, F., Lefkir, Y., Nourrisson, D. & Letourneur, F. (2003). *Dev. Cell*, **5**, 499–511.

Funato, Y. & Miki, H. (2014). *Methods*, **65**, 184–189.

Hendriks, W. J. & Pulido, R. (2013). *Biochim. Biophys. Acta*, **1832**, 1673–1696.

Huang, J., Birmingham, C. L., Shahnazari, S., Shiu, J., Zheng, Y. T., Smith, A. C., Campellone, K. G., Heo, W. D., Gruenheid, S., Meyer, T., Welch, M. D., Ktistakis, N. T., Kim, P. K., Klionsky, D. J. & Brumell, J. H. (2011). *Autophagy*, **7**, 17–26.

Kawahara, T., Quinn, M. T. & Lambeth, J. D. (2007). *BMC Evol. Biol.* **7**, 109.

Kim, S.-A., Taylor, G. S., Torgersen, K. M. & Dixon, J. E. (2002). *J. Biol. Chem.* **277**, 4526–4531.

Kim, S.-A., Vacratsis, P. O., Firestein, R., Cleary, M. L. & Dixon, J. E. (2003). *Proc. Natl Acad. Sci. USA*, **100**, 4492–4497.

Laporte, J., Bedez, F., Bolino, A. & Mandel, J.-L. (2003). *Hum. Mol. Genet.* **12**, R285–R292.

Laporte, J., Biancalana, V., Tanner, S. M., Kress, W., Schneider, V., Wallgren-Pettersson, C., Herger, F., Buj-Bello, A., Blondeau, F., Liechti-Gallati, S. & Mandel, J.-L. (2000). *Hum. Mutat.* **15**, 393–409.

Laporte, J., Blondeau, F., Buj-Bello, A., Tentler, D., Kretz, C., Dahl, N. & Mandel, J.-L. (1998). *Hum. Mol. Genet.* **7**, 1703–1712.

Laporte, J., Hu, L. J., Kretz, C., Mandel, J.-L., Kioschis, P., Coy, J. F., Klauck, S. M., Poustka, A. & Dahl, N. (1996). *Nature Genet.* **13**, 175–182.

Lee, S.-R., Yang, K.-S., Kwon, J., Lee, C., Jeong, W. & Rhee, S. G. (2002). *J. Biol. Chem.* **277**, 20336–20342.

Lemmon, M. A. (2003). *Traffic*, **4**, 201–213.

Lepichon, J.-B., Bittel, D. C., Graf, W. D. & Yu, S. (2010). *Am. J. Med. Genet. A*, **152**A, 1300–1304.

Leslie, N. R., Bennett, D., Lindsay, Y. E., Stewart, H., Gray, A. & Downes, C. P. (2003). *EMBO J.* **22**, 5501–5510.

Lorenzo, Ó., Urbé, S. & Clague, M. J. (2005). *J. Cell Sci.* **118**, 2005–2012.

Lorenzo, Ó., Urbé, S. & Clague, M. J. (2006). *J. Cell Sci.* **119**, 2953–2959.

Matteis, M. A. D. & Godi, A. (2004). *Nature Cell Biol.* **6**, 487–492.

McCoy, A. J., Grosse-Kunstleve, R. W., Storoni, L. C. & Read, R. J. (2005). *Acta Cryst.* **D61**, 458–464.

Mochizuki, Y. & Majerus, P. W. (2003). *Proc. Natl Acad. Sci. USA*, **100**, 9768–9773.

Montfort, R. L. M. van, Congreve, M., Tisi, D., Carr, R. & Jhoti, H. (2003). *Nature (London)*, **423**, 773–777.

Murshudov, G. N., Skubák, P., Lebedev, A. A., Pannu, N. S., Steiner, R. A., Nicholls, R. A., Winn, M. D., Long, F. & Vagin, A. A. (2011). *Acta Cryst.* D**67**, 355–367.

Nandurkar, H. H., Caldwell, K. K., Whisstock, J. C., Layton, M. J., Gaudet, E. A., Norris, F. A., Majerus, P. W. & Mitchell, C. A. (2001). *Proc. Natl Acad. Sci. USA*, **98**, 9499–9504.

Nandurkar, H. H., Layton, M., Laporte, J., Selan, C., Corcoran, L., Caldwell, K. K., Mochizuki, Y., Majerus, P. W. & Mitchell, C. A. (2003). *Proc. Natl Acad. Sci. USA*, **100**, 8660–8665.

Nicot, A.-S. & Laporte, J. (2008). *Traffic*, **9**, 1240–1249.

Odorizzi, G., Babst, M. & Emr, S. D. (2000). *Trends Biochem. Sci.* **25**, 229–235.

Ostman, A., Frijhoff, J., Sandin, A. & Bohmer, F. D. (2011). *J. Biochem.* **150**, 345–356.

Otwinowski, Z. & Minor, W. (1997). *Methods Enzymol.* **276**, 307–326.

Robinson, F. L. & Dixon, J. E. (2006). *Trends Cell Biol.* **16**, 403–412.

Salmeen, A., Andersen, J. N., Myers, M. P., Meng, T.-C., Hinks, J. A., Tonks, N. K. & Barford, D. (2003). *Nature (London)*, **423**, 769–773.

Schaletzky, J., Dove, S. K., Short, B., Lorenzo, O., Clague, M. J. & Barr, F. A. (2003). *Curr. Biol.* **13**, 504–509.

Senderek, J., Bergmann, C., Weber, S., Ketelsen, U. P., Schorle, H., Rudnik-Schöneborn, S., Büttner, R., Buchheim, E. & Zerres, K. (2003). *Hum. Mol. Genet.* **12**, 349–356.

Sivaramakrishnan, S., Cummings, A. H. & Gates, K. S. (2010). *Bioorg. Med. Chem. Lett.* **20**, 444–447.

Sohn, J. & Rudolph, J. (2003). *Biochemistry*, **42**, 10060–10070.

Song, H., Hanlon, N., Brown, N. R., Noble, M. E. M., Johnson, L. N. & Barford, D. (2001). *Mol. Cell*, **7**, 615–626.

Spiro, A. J., Shy, G. M. & Gonatas, N. K. (1966). *Arch. Neurol.* **14**, 1–14.

Storoni, L. C., McCoy, A. J. & Read, R. J. (2004). *Acta Cryst.* D**60**, 432–438.

Tanner, J. J., Parsons, Z. D., Cummings, A. H., Zhou, H. & Gates, K. S. (2011). *Antioxid. Redox Signal.* **15**, 77–97.

Taylor, G. S. & Dixon, J. E. (2003). *Methods Enzymol.* **366**, 43–56.

Tonks, N. K. (2005). *Cell*, **121**, 667–670.

Tosch, V., Rohde, H. M., Tronchere, H., Zanoteli, E., Monroy, N., Kretz, C., Dondaine, N., Payrastre, B., Mandel, J.-L. & Laporte, J. (2006). *Hum. Mol. Genet.* **15**, 3098–3106.

Tsujita, K., Itoh, T., Ijuin, T., Yamamoto, A., Shisheva, A., Laporte, J. & Takenawa, T. (2004). *J. Biol. Chem.* **279**, 13817–13824.

Vergne, I. & Deretic, V. (2010). *FEBS Lett.* **584**, 1313–1318.

Winn, M. D. *et al.* (2011). *Acta Cryst.* D**67**, 235–242.

Wishart, M. J., Taylor, G. S., Slama, J. T. & Dixon, J. E. (2001). *Curr. Opin. Cell Biol.* **13**, 172–181.

Xue, Y., Fares, H., Grant, B., Li, Z., Rose, A. M., Clark, S. G. & Skolnik, E. Y. (2003). *J. Biol. Chem.* **278**, 34380–34386.

Yang, J., Groen, A., Lemeer, S., Jans, A., Slijper, M., Roe, S. M., den Hertog, J. & Barford, D. (2007). *Biochemistry*, **46**, 709–719.

Zhang, Z. Y. & Dixon, J. E. (1993). *Biochemistry*, **32**, 9340–9345.

Zou, J., Chang, S.-C., Marjanovic, J. & Majerus, P. W. (2009). *J. Biol. Chem.* **284**, 2064–2071.